

Differences of interface and bulk transport properties in polymer field-effect devices

S. Grecu, M. Roggenbuck, A. Opitz, W. Brütting

Experimentalphysik IV, Universität Augsburg, 86135 Augsburg, Germany

Abstract

The influence of substrate treatment with self-assembled monolayers and thermal annealing was analysed by electrical and structural measurements on field-effect transistors (FETs) and metal-insulator-semiconductor (MIS) diodes using poly(3-hexylthiophene) (P3HT) as a semiconducting polymer and Si/SiO₂ wafers as a substrate.

It is found that surface treatment using silanising agents like hexamethyldisilazane (HMDS) and octadecyltrichlorosilane (OTS) can increase the field-effect mobility by up to a factor of 50, reaching values in saturation of more than 4×10^{-2} cm²/Vs at room temperature. While there is a clear correlation between the obtained field-effect mobility and the contact angle of water on the treated substrates, X-ray diffraction and capacitance measurements on MIS diodes show that structural and electrical properties in the bulk of the P3HT films are not influenced by the surface treatment. On the other hand, thermal annealing is found to cause an increase of grain size, bulk relaxation frequency and thereby of the mobility perpendicular to the SiO₂/P3HT interface, but has very little influence on the field-effect mobility. Temperature dependent investigations on MIS diodes and FETs show that the transport perpendicular to the substrate plane is thermally activated and can be described by hopping in a Gaussian density of states, whereas the field-effect mobility in the substrate plane is almost temperature independent over a wide range. This investigations reveal significant differences between interface and bulk transport properties in polymer field-effect devices.

PACS: 61.41.+e ; 61.10.Eq; 72.80.Le; 73.61.Ph; 82.35.Gh

Keywords: Organic transistor; MIS diode; Self-assembled monolayer; Polythiophene; P3HT

1. Introduction

In recent years conjugated polymers have gained increasing interest as active materials in organic electronics. Their wide range of chemical variability in combination with low-cost solution processing make them attractive candidates for the fabrication of electronic devices such as light-emitting diodes (LEDs), photovoltaic cells (PVCs) and field-effect transistors (FETs)^{1,2}. For the latter, high field-effect mobility is required and this is usually associated with high degree of structural order of the films. Poly(alkylthiophenes) have proven to be very promising candidates to achieve this goal. Charge carrier mobility as high as 0.1 cm²/Vs has been reported in regio-regular poly(3-hexylthiophene) (rr-P3HT)³, its structure being shown in Fig. 1.

In field-effect transistors the charge transport in the active channel is restricted to a few monolayers close to the interface⁴, so it is to be expected that the surface treatment of the underlying substrate has a strong influence on the charge carrier mobility of P3HT FETs⁵. Another issue that comes into play is the anisotropy of charge carrier transport in polymeric field-effect devices. The regular arrangement of the alkane side groups promotes the formation of a lamellar stacking of the polymer chains with good π -orbital overlap between neighboring chains. This orientation, results in anisotropy of the mobility in the parallel and perpendicular direction with respect to the substrate. From the comparison of MIS diodes and FET data Scheinert *et al.*⁶ and our group⁷ have suggested that the charge carrier mobility in the substrate plane and perpendicular to it may differ by up to four orders of magnitude. Contrarily, Tanase *et al.*⁸ have shown that differences between the values of the field-effect mobility and the values obtained from space-charge limited currents in diode structures is due to a charge carrier density dependence of the mobility in disordered hopping systems. In amorphous films of OC₁C₁₀-PPV and P3HT having field-effect mobility in the range 10⁻⁵-10⁻⁴ cm²/Vs, at room temperature, no evidence for a pronounced anisotropy of charge carrier transport was found.

In this paper we will demonstrate that by suitable substrate treatment the field-effect mobility of P3HT can be varied over a large range whereby the surface energy of the Si/SiO₂ substrate will turn out to be the decisive control parameter. We will further show that by silanisation highly ordered films with field-effect mobility approaching 0.1 cm²/Vs can be achieved in which the transport mechanism in the substrate plane and perpendicular to it is fundamentally different.

2. Experimental

2.1. Sample preparation

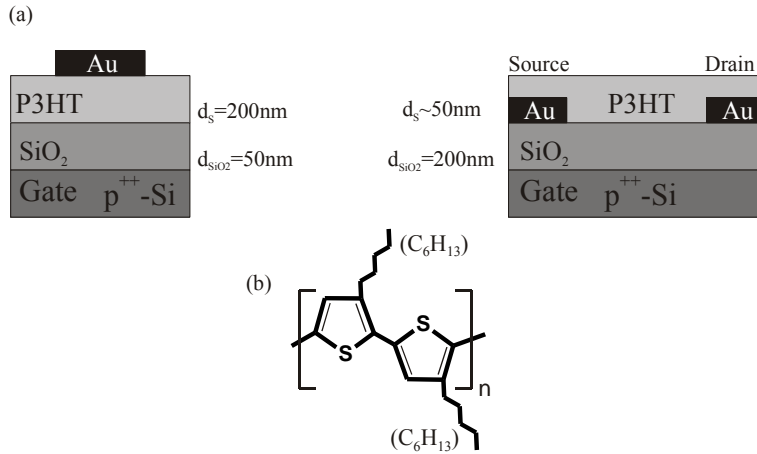


Fig. 1: (a) Device structure of MIS diode and field-effect transistor, (b) Chemical structure of regioregular poly(3-hexylthiophene)

The substrates used in this work were highly p-doped Si wafers (1-5 mΩ cm) with high quality, thermally grown oxide as the gate insulator. Four different types of surface treatments were employed prior to the deposition of P3HT. The first substrate type was only wet-cleaned in an ultrasonic bath with solvents (acetone, isopropanol), in the following termed untreated. The other three were additionally exposed to oxygen plasma in order to create a hydrophilic surface which is required for the growth of self assembled monolayers through a silanisation reaction. One of these substrates, to which we will refer to as the O₂ plasma treated one, was used to prepare field-effect devices without any further treatment. The other two were used for silanisation immediately after the O₂ plasma treatment. Two types of silane molecules, hexamethyldisilazane (HMDS) and octadecyltrichlorosilane (OTS), respectively, were used. The HMDS treatment was done in the liquid phase at 60°C for 24 hours. The OTS treatment was carried out at room temperature, in a solution of OTS in n-heptane (0.86mM), in an exsiccator. Samples were subsequently cleaned from residual OTS in chloroform in an ultrasonic bath. The values of the contact angles of water droplets on these substrates are summarized in Table 1.

Table 1: Contact angles of water for the different types of samples

Sample Type	O ₂ plasma	Untreated	HMDS	OTS
Contact Angle(°)	<5	60±2	95±1	110±1

The MIS diodes have been prepared on Si substrates with a 50nm thin oxide layer (Fig. 1). Solutions of regioregular P3HT in toluene (5 %wt.) were spin-coated at 2000rpm resulting in films with a thickness of about 250-300nm, except for the O₂ sample where it was about 130nm. The P3HT was obtained from Merck and used without any additional purification. The molecular weight of P3HT was about 14,000. After a drying step (12h, 10⁻³ Torr, 330K), for all samples, top gold contacts were evaporated through a shadow mask, defining an area of about 25-30mm². The FETs were prepared by spin-coating a 50nm thick P3HT film onto Si/SiO₂ substrates with photolithographically patterned source and drain electrodes from Au, having a circular geometry to reduce leakage currents. The insulator thickness was 200nm, the channel width 5μm and channel length 1000μm. Thus, the resulting FETs were in the bottom-gate, bottom-contact configuration (Fig. 1). To avoid unintentional doping by oxygen the whole film preparation was performed in a glove-box system under inert atmosphere (<0.1ppm oxygen and <1ppm water content). The substrates for the X-Ray diffraction analysis were normal glass. In this case the P3HT films were spin-coated from a 5%wt. solution in toluene at 1000rpm resulting in a thickness of about 400-450nm. Additionally, heating at 350K in high vacuum was applied to the samples in order to study the influence of further thermal annealing.

2.2. Measurement details

The X-ray diffraction (XRD) measurements were performed on a Siemens D-5000 diffractometer in grazing incidence geometry (0.03° between the incident beam and the sample, wavelength 1.54Å), on pristine and annealed films for all types of samples.

The MIS diodes were characterized by measuring the capacitance–voltage (C – V) and capacitance–frequency (C – f) dependence, using a Solartron 1260 impedance/gain-phase analyzer coupled with a Solartron 1296 dielectric interface, in the frequency range from 1 to 10^6 Hz. An a.c. amplitude of 0.5V and bias between -10V and +10V was used to operate the diodes either in accumulation or depletion. Measurements of the output and transfer characteristics of FETs were performed using two independent source-measure units (Keithley 236). Both types of devices were measured and annealed in a cryostat in high vacuum ($<10^{-6}$ mbar) and darkness. The transfer between the glove-box and the cryostat was performed in a load-lock system so that the samples were not exposed to air.

3. Results and discussion

3.1. Structural investigations

The structural ordering of the P3HT films was analysed by XRD measurements. P3HT films were prepared on untreated as well as O_2 plasma, HMDS and OTS treated substrates, as previously mentioned. Additionally the changes upon thermal annealing of the films (up to 24h, 350K) were analysed. The XRD spectra of the P3HT films deposited after different surface treatments are shown in Fig. 2(a). The effect of thermal annealing is shown as an example for the untreated substrate in Fig. 2(b).

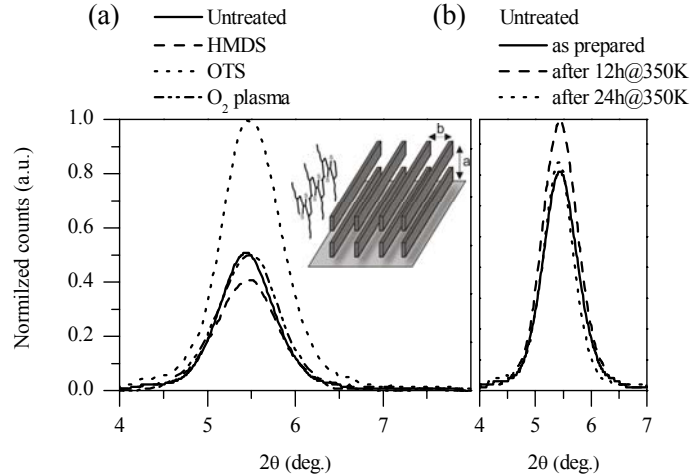


Fig. 2: Gracing incidence x-ray diffraction patterns of P3HT films on Si/SiO₂ substrate. (a) P3HT on substrates prepared by different surface treatments. The inset shows a cartoon of the lamellar structure and layer spacing. (b) XRD peak of P3HT on an untreated substrate before and after annealing for 12 h at 350 K.

The observed first order diffraction peaks were fitted in order to calculate the lattice constant a from the Bragg condition

$$2a \sin(\theta) = n\lambda$$

The crystallite size l was obtained from the Scherrer equation using the relation between full width at half maximum $FWHM$ (2θ) of the diffraction peak and the diffraction angle 2θ

$$FWHM(2\theta) = 0.94 \cdot \lambda / l \cdot \cos(\theta).$$

All spectra show a diffraction peak at about 5.4° which is known for the organized lamellar structure of rr-P3HT with π - π -interchain stacking. This corresponds to a layer spacing for the (100) direction of $a=16.1\pm0.2$ nm, which is comparable to literature data⁹. No evidence for the other two possible orientations of P3HT with respect to the substrate (corresponding to diffraction peaks around 23°) was found³.

The layers spacing and crystallite sizes, determined after extracting the background signal and the $K\alpha_2$ peak, are summarized in Table 2. Within the error limit, the layer spacing is the same for the different substrate treatments and stays constant during annealing. The effect of annealing on the degree of crystallinity cannot be estimated from x-ray diffraction, as the intensity of the diffraction peak, to which it should be proportional, varies from sample to sample without any correlation. A possible explanation of this behaviour could be the reorientation of the P3HT lamellae in the bulk, as

the grazing incidence method is sensitive only to the ones perpendicular to the substrate and x-ray beam. What is to be remarked is the decrease of the FWHM, as shown in Fig. 2b, meaning that the size of crystalline domains increases upon annealing.

Table 2: Layer spacing and grain size of P3HT films determined by gracing incidence x-ray diffraction for different substrate treatments and thermal annealing.			
Treatment		Layer spacing [Å]	Crystallite size [nm]
Untreated	As prepared	16.21	10.61
	After annealing	16.22	12.82
HMDS	As prepared	16.22	10.96
	After annealing	16.07	11.01
OTS	As prepared	16.07	10.10
	After annealing	15.90	11.74
O_2 plasma	As prepared	16.08	9.62
	After annealing	16.17	10.24

3.2. Measurements on MIS diodes

Capacitance-frequency and capacitance-voltage measurements were performed on MIS diodes prepared with different substrate treatment (Fig. 3 and 4). In general, the C - V of p-conducting organic MIS diodes shows two regimes: accumulation at negative bias and depletion at positive bias with the measured value of C corresponding either to the oxide capacitance or to the series sum of the oxide capacitance and the depletion capacitance in the organic semiconductor, respectively. The absence of inversion is explained by the extraordinarily long generation times for minority carriers in wide-gap organic semiconductors^{10,11}.

Using the standard Schottky–Mott analysis, the doping concentration N_A can be extracted from the slope of the C - V curves in the transition region between C_{\max} and C_{\min} via¹²

$$\frac{\partial}{\partial V} (C^{-2}) = \frac{2}{\varepsilon_0 \varepsilon_S q N_A A^2},$$

where ε_0 is the permittivity of vacuum, ε_S the dielectric constant of the insulator and A the active diode area. Thus N_A can be extracted from a plot of $1/C^2$ vs. the voltage applied to the Si bottom gate electrode as shown in Fig. 4 for two significant samples.

The C - f curves measured at negative gate bias show a relaxation step from the accumulation capacitance to the lower value in depletion. The reason is the finite semiconductor bulk conductivity which sets an upper limit for the frequency up to which the injected majority carriers can follow the applied a.c. frequency and reach the accumulation layer at the interface to the oxide. The C - f measurements were modelled by the equivalent circuit shown in the inset of Fig. 3 as a series of insulator (R_{ins} , C_{ins}), semiconductor (R_S , C_S) and contact or lead resistance (R_L). For $R_{\text{ins}} \gg R_S$ the relaxation time τ_R is given by

$$\tau_R = R_S (C_{\text{ins}} + C_S).$$

On the one hand, it is required that the frequency for analyzing the C - V curves is much lower than the relaxation frequency $f_R = (2\pi \tau_R)^{-1}$. On the other hand, f_R can be used to determine the bulk semiconductor resistance R_S (which is directly obtained as a fit parameter in modelling of the C - f curves with the depicted equivalent circuit). With the knowledge of the doping concentration N_A from the C - V analysis one can then calculate the charge carrier mobility μ_{\perp} perpendicular to the insulator via:

$$R_S = \frac{d_S}{q N_A \mu_{\perp} A}.$$

The experimental C - f curves are shown for the different samples in Fig. 3. The oxide capacitance is about 20 nF. The increase of C beyond this value at low frequencies is related to spreading effects because in the actual device the area of

the lower contact and the polymer film are much larger than the area of the top contact. In Figure 3 one can notice two important things. On the one hand, substrate treatment has only a weak influence on the relaxation frequency, but on the other hand there is a strong effect of annealing on it. Whereas the pristine MIS diodes show relaxation frequencies in the range of 10 to 100Hz the annealed devices have significantly higher values of f_R in the kHz range (see Table 3). This clearly indicates that the semiconductor bulk resistance in MIS diodes can be drastically reduced by up to three orders of magnitude by thermal annealing, whereas substrate treatment has only a weak influence on it.

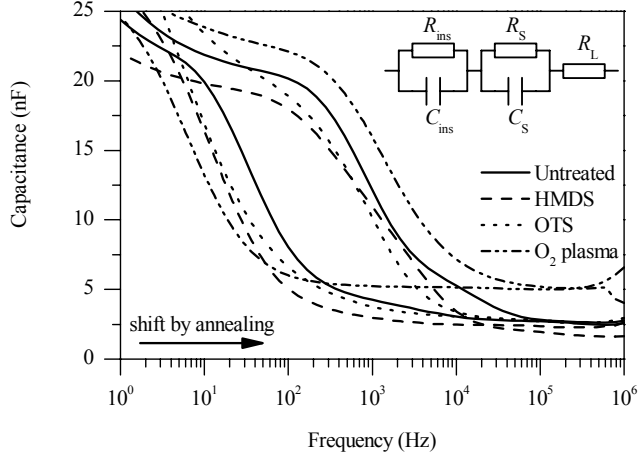


Fig. 3: Capacitance-frequency characteristics of Au/P3HT/SiO₂/Si MIS diodes for different substrate treatments before and after annealing for 24h at 350 K. The diodes were measured in the accumulation regime with -10V at the Si contact. The inset shows an equivalent circuit containing resistors and capacitors for contacts, semiconductor and insulator.

Since the changes in doping upon annealing as determined from the C - V data are comparatively small (see below) one has to conclude that the charge carrier mobility perpendicular to the insulator interface is strongly enhanced by annealing and can be correlated with the increase of the grain size, as seen in the X-Ray diffraction measurement. The calculated values are summarized in Table 3.

Table 3: MIS diode parameters (relaxation frequency f_R , doping concentration N_A , mobility perpendicular to the interface μ_\perp) for different substrate treatments and thermal annealing.				
Treatment		f_R	N_A	μ_\perp
Untreated	As prepared	35	2.5×10^{15}	1.9×10^{-7}
	After annealing	840	5.7×10^{15}	2.0×10^{-6}
HMDS	As prepared	10	2.1×10^{15}	6.5×10^{-8}
	After annealing	1135	1.7×10^{15}	9.2×10^{-6}
OTS	As prepared	10	5.6×10^{15}	2.4×10^{-8}
	After annealing	774	4.6×10^{15}	2.3×10^{-6}
O_2 plasma	As prepared	6	2.5×10^{16}	2.5×10^{-9}
	After annealing	1450	3.2×10^{16}	4.7×10^{-7}

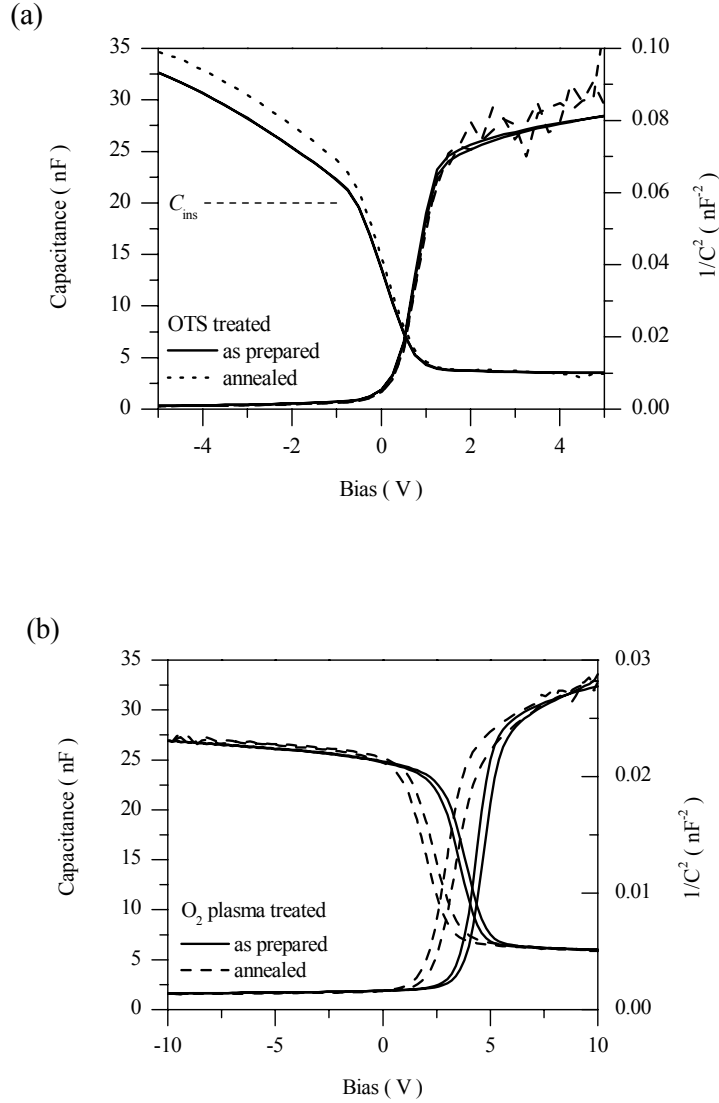


Fig. 4: Capacitance-voltage characteristics of Au/P3HT/SiO₂/Si MIS diodes for different substrate treatments before and after annealing for 24h at 350 K.

The C - V curves of the different samples are shown in Fig. 4. From the Schottky-Mott analysis very similar doping concentrations in the range $2\text{--}6 \times 10^{15} \text{ cm}^{-3}$ are obtained for all samples, with the exception of the O₂ plasma treated one, where N_A is one order of magnitude higher (see Table 3). A closer look at the C - V curves reveals some interesting details: Whereas the untreated, HMDS (both not shown) and OTS-treated MIS diodes show a sharp transition between accumulation and depletion at zero or slightly positive voltage with only marginal hysteresis between increasing and decreasing bias sweeps, the O₂ plasma treated diode has a larger hysteretic behaviour and the transition between accumulation and depletiton takes place at higher biases (between 2.5 and 5V). This can be seen as an indication of interface states at the P3HT/SiO₂ interface created by the O₂ plasma treatment. In the case of the OTS-treated surface the capacitance does not saturate at the oxide capacitance value in the accumulation regime, but increases significantly above the expected value. This can be explained by charge spreading beyond the active area defined by the top contact¹³ which can be seen as an indication for high in-plane charge carrier mobility parallel to the oxide surface for this substrate type (see below). Similar, smaller, increase can be seen for the other samples, too.

3.3. Measurements on OFETs

The output and transfer characteristics of bottom-gate bottom-contact FETs for the different treatments of SiO_2 substrates are shown in Fig. 5. The output characteristics (Fig. 5a) show a linear onset with little evidence for contact resistances and a well-defined saturation region for $|V_D| > |V_G|$. As seen from the output characteristics, at a given gate voltage (-10V), the current increases, from the untreated substrate towards the OTS-treated one, by more than one order of magnitude. This can either be caused by an increase of the charge carrier mobility or/and by a positive shift of the threshold voltage. Therefore one has to look at the transfer characteristics in more detail. The semi logarithmic plot (Fig. 5b) allows for the extraction of the ON-OFF ratio and the switch-on voltage V_{so} whereas a plot of $\sqrt{I_D}$ vs. V_G (Fig. 5c) yields the field-effect mobility μ and the threshold voltage V_T in the saturation regime according to

$$I_{D,\text{Sat}} = \frac{W}{2L} \mu \cdot C_{\text{ins}} (V_G - V_T)^2.$$

Therein W and L are the channel width and channel length, respectively, C_{ins} is the specific capacitance of the oxide, V_G is the gate voltage and V_T the threshold voltage. The resulting parameters for the four different substrate treatments before and after annealing are summarized in Table 4.

Table 4: OFET parameters (mobility μ_{sat} , switch-on voltage V_{so} , threshold voltage V_T , ON/OFF ratio and inverse subthreshold slope S) for different surface treatments as well as before and after thermal annealing.						
Treatment		μ_{sat} [cm ² /Vs]	V_T [V]	V_{so} [V]	ON/OFF	S [V/dec]
Untreated	As prepared	1.7×10^{-3}	-6.34	-4.06	1.2×10^7	0.44
	After annealing	2.2×10^{-3}	-2.90	-0.65	2.6×10^7	0.36
HMDS	As prepared	1.3×10^{-2}	-0.20	7.50	7.8×10^7	1.56
	After annealing	1.3×10^{-2}	0.90	9.50	1.9×10^7	0.85
OTS	As prepared	3.4×10^{-2}	-2.30	3.65	1.4×10^6	0.92
	After annealing	4.1×10^{-2}	-2.75	1.52	1.7×10^7	0.62
O_2 plasma	As prepared	8.4×10^{-4}	3.81	6.25	3×10^6	0.60
	After annealing	8.7×10^{-4}	12.64	10	4×10^7	0.49

Comparing the different treatments the most striking difference is the increase of μ by about 40 times from the O_2 plasma substrate to the OTS-treated one before annealing (after annealing the increase is approximately 50). At the same time, the FET on the untreated substrate has the highest ON-OFF ratio, the most negative threshold voltage, and the lowest value of the inverse subthreshold slope. The ON-OFF ratio for the OTS-treatment is significantly lower but still acceptable. The HMDS-treated substrate has a high threshold voltage and also a high value of the inverse subthreshold slope. The highest value of V_T , however, is found for the O_2 plasma treated sample.

After thermal annealing the transfer characteristics show a shift of the switch-on and threshold voltage the magnitude and direction of the shift are not the same for all the samples. The FET on the untreated substrate shows a positive shift, whereas the shift for the OTS treated sample is smaller and negative. The HMDS treated FET is almost unchanged (see Table 4), while the V_T of the O_2 sample increases dramatically. Further, the ON-OFF ratio and the inverse subthreshold slope are slightly improved by thermal annealing. Most remarkable, however, is the fact there is no significant change in the field-effect mobility, reflected by the slopes of the curves in Fig. 5c.

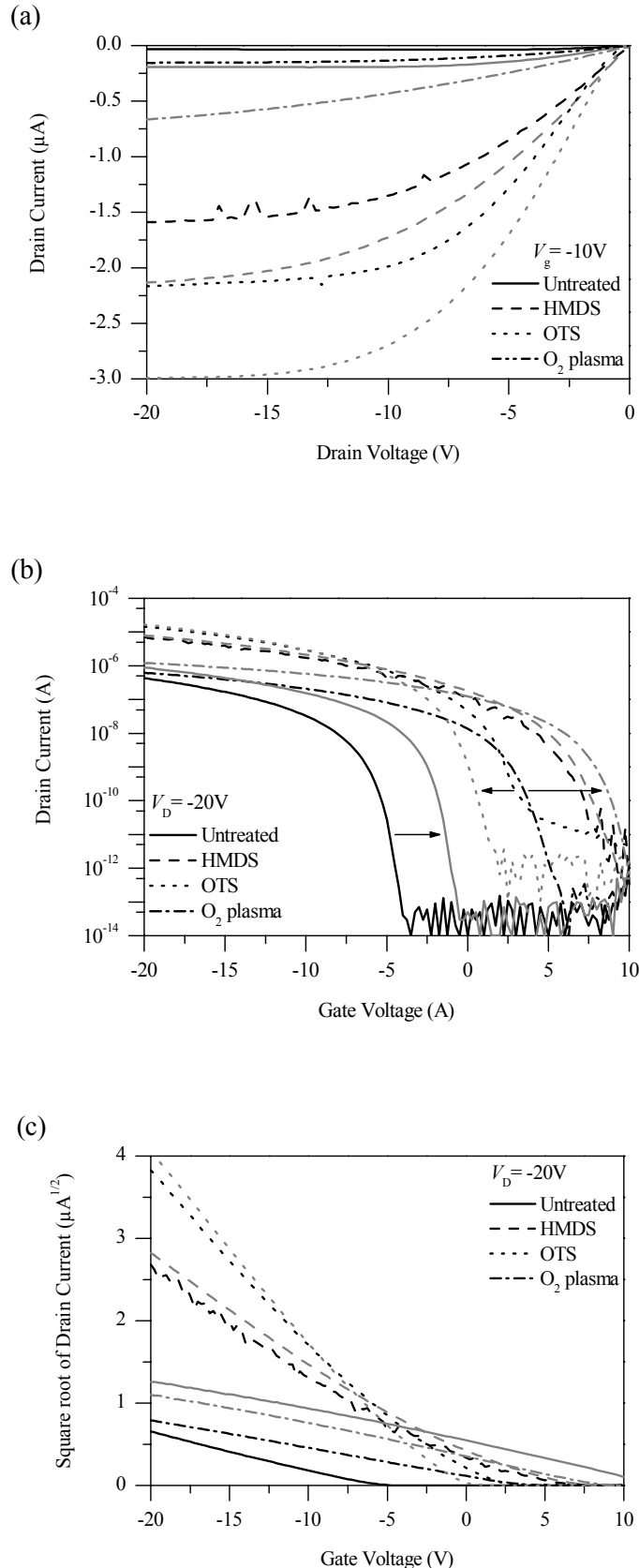


Fig. 5: (a) Output characteristics and (b, c) transfer characteristics of P3HT field-effect transistors with different substrate treatments before and after thermal annealing. The black curve is the initial one and the grey curve after annealing. The change is marked in Fig (b) by an arrow, except for the HMDS treatment. The transfer characteristics are shown on semi-logarithmic scale (b) and as the square root of the drain current (c).

3.4. Temperature dependence of MIS diode and FET characteristics

In order to get further insight into the transport mechanism in the substrate plane and perpendicular to it, we measured the temperature dependence of the $C-f$ characteristics in MIS diodes and the transfer characteristics in FETs. The obtained curves in the temperature range between 200 and 420K are shown in Fig. 6 for the OTS treated substrates. As shown in Fig. 6a, the bulk relaxation frequency in the MIS diode shifts over almost four orders of magnitude in the investigated temperature range. Since no significant change of the doping concentration in MIS diodes was observed, this strong shift of f_R directly reflects a strong temperature dependence of the perpendicular mobility in MIS diodes. Contrarily, in FETs (see Fig. 6b) the current at large gate voltage changes by only a factor of two over the whole temperature range indicating a very weak temperature dependence of the field-effect mobility parallel to the substrate. Even if the temperature is lowered to 40K (not shown here) the mobility stays at about $1 \times 10^{-2} \text{ cm}^2/\text{Vs}$.

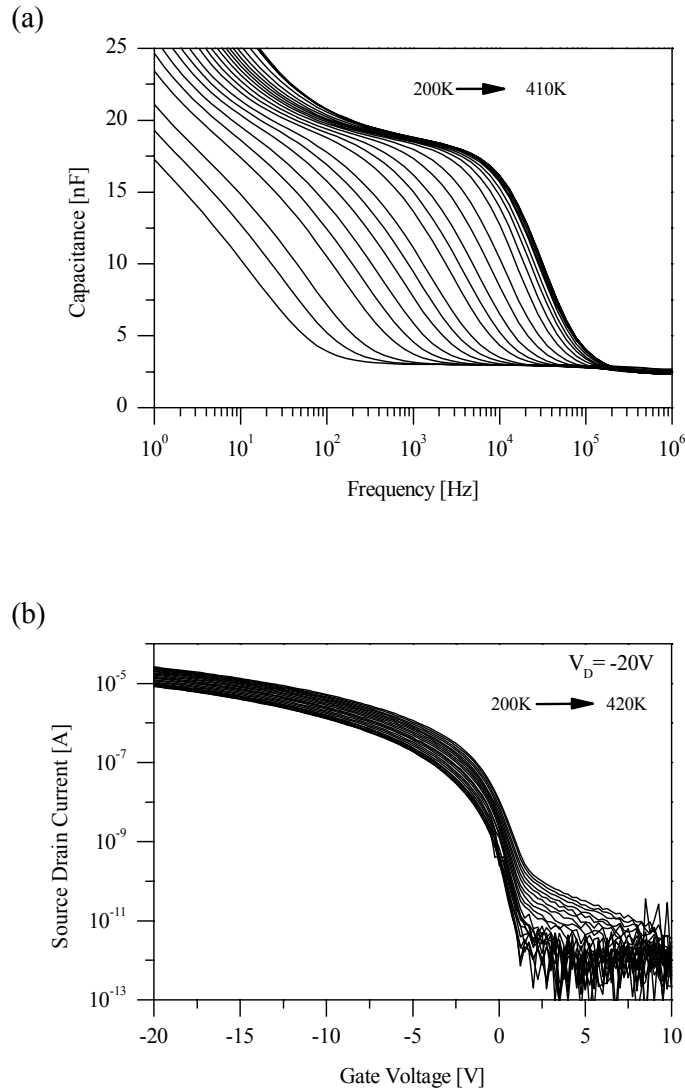


Fig. 6: Temperature dependence of MIS diode and FET characteristics of samples with OTS treated substrates and thermal annealing at 420K, measured from 200 to 410K in steps of 10K: (a) $C-f$ characteristics in accumulation, (b) transfer characteristics in saturation.

In Figure 7 the temperature dependence of the mobility for MIS diodes and field-effect transistors on the different substrates is shown. Among the different substrates, the temperature dependence of the field-effect mobility is weakest for the OTS treatment which also results in the highest values at all temperatures. For the other samples, with smaller values of the field-effect mobility, the temperature dependence is somewhat stronger, but still less than one order of magnitude.

By contrast, the change of the mobility in MIS diodes amounts to several orders of magnitude, for all the samples, and shows the typical behaviour of hopping transport in a Gaussian density of states. Considering the correlated disorder model¹⁴, where the expression for the field-effect mobility, in the small electric field approximation, is given by

$$\mu(E \rightarrow 0) = \mu_0 \exp \left[- \left(\frac{3\sigma}{5kT} \right)^2 \right]$$

with σ the width of Gaussian DOS, k Boltzmann's constant, T absolute temperature and μ_0 absolute mobility. Values for σ of 98meV for the OTS treated MIS diode, 118meV for the HMDS treated one, 110meV for the O₂ treated one and 105meV for the untreated substrate are obtained. As σ is a measure of disorder in the system, it indicates that the films on the OTS treated substrate have the lowest degree of disorder, while the HMDS ones have the highest degree of disorder. The observed decrease of mobility above 380K for the untreated, HMDS and OTS treated substrates is probably due to morphological changes rather than thermal degradation of the polymer. The O₂ treated sample, however, shows a steep increase of the perpendicular mobility at temperatures above 335K, which could be related to oxygen doping or morphological changes at the oxygen plasma treated SiO₂-P3HT interface upon annealing at higher temperatures. This indicates that this substrate treatment is less stable as compared to the other three methods.

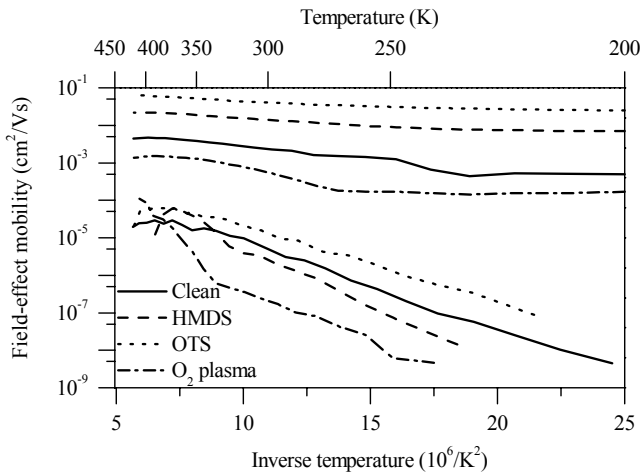


Fig. 7: Temperature dependence of the field-effect mobility and the mobility from the bulk relaxation time in MIS diodes for different substrate treatments. The plot vs. $1/T^2$ is in accordance with the correlated disorder model.

3.4. Discussion

In this work, we have addressed interface and bulk transport in polymeric field-effect devices. We have seen significant differences between the field-effect mobility parallel to the polymer-SiO₂ interface and the mobility perpendicular to it. The room temperature mobility values in MIS diodes and FETs for different treatments are listed in tables 3 and 4. The values are distinguished by surface treatment, which is characterized by a distinct contact angle, as well as by thermal treatment. Clearly, the field-effect mobility increases by almost two orders of magnitude with the surface treatment, but does not change very much due to thermal annealing over the measured temperature range. Contrarily, the perpendicular mobility in MIS diodes increases upon thermal annealing by up to four orders of magnitude and becomes almost independent of the substrate treatment.

Thus, the effect of substrate treatment and thermal annealing is almost complementary in FETs and MIS diodes. While the field-effect mobility for charge carrier transport along the surface is mainly affected by surface treatment, the mobility of MIS diodes perpendicular to the surface can be enhanced strongly by thermal annealing. The latter can be correlated to the increase in crystallinity in the bulk of the films, as seen from XRD measurements, which should result in an improved interchain hopping of carriers perpendicular to the substrate. Additionally, the doping profile might become more homogeneous during annealing, although the $1/C^2$ vs. V plot do not show significant changes going in that direction.

Interestingly, the field-effect mobility shows a close correlation with the water contact angle on the substrate, increasing with the hydrophobicity of the SiO₂ surface. Such behaviour has recently also been observed by Veres *et al.*⁵. Fig. 8 shows their data together with the values obtained in this work. The excellent agreement is remarkable, with the excep-

tion of the O_2 plasma treated FET. However, this may be related to the fact that the O_2 plasma treatment additionally causes acceptor-like doping of the P3HT layer, which can enhance the observed mobility¹⁵. Veres et al. have probably used surface treatments with polar SAMs to achieve low contact angles, so that this effect did not occur in their work. Thus one has to conclude that the modification of the surface energy of silicon oxide by appropriate treatments is of outmost importance for achieving high field-effect mobilities in OFETs with P3HT as a semiconducting polymer. As an explanation one can take the suggested lamellar structure of the P3HT chains (see. Fig. 2) in which the aliphatic side chains are standing upright on the substrate. Obviously, this structural motive within the first few monolayers is crucial for achieving good π - π -interchain stacking and thus high charge carrier mobility parallel to the surface of the SiO_2 gate dielectric. From our XRD and MIS diode measurements, however, one has to conclude that the improved interfacial ordering achieved by substrate treatment with silanising agents does not extend through the whole of the P3HT film. Thus the structural properties of the bulk of P3HT which are probed by XRD measurements are not directly correlated to the field-effect mobility. This is in agreement with the results on thermally annealed films, where structural data indicate an increase grain size, but no significant change of the field-effect mobility is observed.

These results are in going with recent publications on the charge carrier distribution within the active channel of organic FETs. Tanase et al. have shown that in disordered organic FETs the charge carrier density decreases already by an order of magnitude within the first nanometers away from the gate dielectric¹⁶. Taking into account the carrier density dependence of the mobility in disordered systems they could show that the macroscopically measured field-effect mobility corresponds to the local mobility of charge carriers directly at the interface. By performing in-situ electrical measurements during layer growth Dinelli et al. came to a similar result for FETs with ordered layers of sexithienyl molecules¹⁷. They could show that the first two monolayers next to the dielectric interface dominate the charge transport.

Therefore, it is understandable that the substrate treatment in bottom-gate FETs, based on rr-P3HT, has such a strong influence on the field-effect mobility. As shown in Fig. 8, the mobility can be varied over three orders of magnitude when the surface of the SiO_2 gate insulator is changed from a hydrophilic to an extremely hydrophobic one. If this crucial parameter is not properly controlled in the experiment, large scattering of the field-effect mobility can be obtained in nominally identical devices (see e.g. the compilation of data from different groups in Ref. 5). Further consequences of different surface treatments are seen in variations of related transistor parameters such as switch-on or threshold voltage, ON-OFF ratio and subthreshold slope. Pernstich et al. have recently published a comprehensive survey of these effects in pentacene FETs¹⁸. Although we have not studied these effects in detail, our data show that substrate treatment also has a strong influence on these parameters. Their control will be crucial for fabricating electronic circuits based on organic FETs.

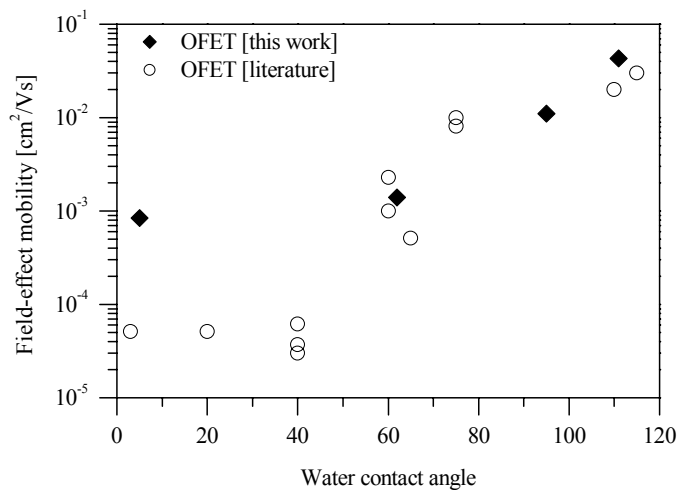


Fig. 8: Field-effect mobility vs. water contact angle for different surface treatments of the SiO_2 insulator. The data shown as open circles are taken from Ref. 5.

Another outcome of our work is the huge difference of charge carrier mobility for OFETs and MIS-diodes. The perpendicular mobility is orders of magnitude smaller than the field-effect mobility parallel to the interface even after thermal annealing. Such differences between in-plane and sandwich geometry have been observed before on polymeric devices^{6,8,16}. However, there was a debate whether this difference is due to a structural and electrical anisotropy of the polymer film or a consequence of the mobility depending on the carrier density. As Tanase *et al.*⁴ have demonstrated by a comparison of FET mobility data with mobility data obtained from space-charge limited currents on diodes an apparent anisotropy of about a factor of 10 could be explained in amorphous polymers by the latter effect. Nevertheless, they

also found that in ordered polymers (e.g. OC₁₀C₁₀-PPV) there exists a true electrical anisotropy which is not explained by different carrier densities in OFETs and diodes⁴. For the case of P3HT, they have observed FET mobility up to $6 \times 10^{-4} \text{ cm}^2/\text{Vs}$ at $V_G = -19\text{V}$ which is almost two orders of magnitude lower than the mobilities obtained here on silanised substrates. Thus it is questionable whether P3HT as prepared here can be treated as an amorphous polymer. The XRD data rather indicate that our P3HT films are nanocrystalline. We therefore suggest that the observed huge differences between the mobilities for transport parallel and perpendicular to the gate insulator interface are caused by a structural anisotropy. Preliminary ellipsometric measurements on our P3HT films have also indicated considerable optical anisotropy in P3HT comparable to poly(3-octylthiophene)¹⁹.

Moreover, the most convincing argument for a true electrical anisotropy of P3HT films comes from our temperature dependent investigations on MIS diodes and FETs. The temperature dependent mobility data for both types of devices (see Fig. 7), clearly shows that charge carrier transport parallel and perpendicular to the dielectric interface is governed by different mechanisms. The perpendicular mobility is well described by hopping in a Gaussian DOS and the obtained values of the disorder parameter σ are in the typical range of disordered polymers^{8,20}. Contrarily, the temperature dependence of the field-effect mobility parallel to the gate is extremely weak and obviously not described by hopping transport. On the other hand, the field-effect mobility is still decreasing with decreasing temperature so that band transport also has to be ruled out. We therefore suggest that silanisation of SiO₂ leads to a highly ordered lamellar structure of the P3HT film within the first few monolayers where the charge carrier transport is in the intermediate range between hopping and band transport. We note that a recently published model for transport in polycrystalline polymer thin-film transistors¹¹ is also not able to account for the observed weak temperature dependence of the FET mobility obtained here. Thus further work will be needed to describe charge transport in this regime.

4. Conclusion

In conclusion, we have found that the mobility in P3HT field-effect transistors depends very sensitively on the nature of the interface to the gate dielectric. Using silanisation of SiO₂ with different agents the mobility can be increased by almost two orders of magnitude and reaches values of about $4 \times 10^{-2} \text{ cm}^2/\text{Vs}$. Interestingly, the structural ordering in the bulk of the films as controlled by thermal annealing has almost no influence on the field-effect mobility.

By comparing OFETs with MIS diodes we have found a strong anisotropy of charge carrier transport parallel and perpendicular to the gate dielectric which is ascribed to the lamellar structure of P3HT chains on SiO₂ substrates. As a consequence, highly ordered P3HT films display hopping transport in the perpendicular direction, whereas in the film plane an almost temperature independent transport is observed.

5. Acknowledgment

This work was supported by the Deutsche Forschungsgemeinschaft (Focus Programme "Organic Field-Effect Transistors") and the German Bundesministerium für Bildung und Forschung (Focus Programme "Polymer Electronics", POLITAG project). We thank Dago de Leeuw and Maxim Skhunov for helpful discussions and the companies Merck and Philips for providing materials and financial support.

References

- ¹ R.H. Friend, R.W. Gymer, A.B. Holmes, J.H. Burroughes, R.N. Marks, C. Taliani, D.D.C. Bradley, D.A. Dos Santos, J.L. Brédas, M. Lögglund, W.R. Salaneck, *Nature* **397** (1999) 121.
- ² C.J. Brabec, C. Winder, N.S. Sariciftci, J.C. Hummelen, A. Dhanabalan, P.A. van Hal, R.A.J. Janssen, *Adv. Func. Mat.* **12** (2002) 709.
- ³ H. Sirringhaus, P.J. Brown, R.H. Friend, M.M. Nielsen, K. Bechgaard, B.M.W. Langeveld-Voss, A.J.H. Spiering, R.A.J. Janssen, E.W. Meijer, P. Herwig, D.M. de Leeuw, *Nature* **401** (1999) 1038.
- ⁴ C. Tanase, P.W.M. Blom, D.M. de Leeuw, E.J. Meijer, *phys. stat. sol. (a)* **201** (2004) 1236.
- ⁵ J. Veres, S. Ogier, G. Lloyd, D. de Leeuw, *Chem. Mater.* **16** (2004) 4543.
- ⁶ S. Scheinert, W. Schlieffke, *Synth. Met.* **139** (2003) 501.
- ⁷ S. Grecu, M. Bronner, A. Opitz, W. Brütting, *Synth. Metals* **146** (2004) 359.
- ⁸ C. Tanase, E.J. Meijer, P.W.M. Blom, D.M. de Leeuw, *Phys. Rev. B* **91** (2003) 216601.
- ⁹ T.J. Prosa, M.J. Winokur, J. Moulton, P. Smith, A.J. Heeger, *Macromolecules* **25** (1992) 4363.
- ¹⁰ S. Scheinert, G. Paasch, *phys. stat. pol. (a)* **201** (2004) 1263.
- ¹¹ R.A. Street, J.E. Northrup, A. Salleo, *Phys. Rev. B* **71** (2005) 165202.
- ¹² S.M. Sze, *Physics of Semiconductor Devices*, Wiley, New York, 1982.
- ¹³ S. Ogawa, Y. Kimura, H. Ishii, M. Niwano, *Jpn. J. Appl. Phys.* **42** (2003) L1275.
- ¹⁴ P.W.M. Blom, M.C.J.M. Vissenberg, *Mater. Sci. Eng.* **27** (2000) 53.
- ¹⁵ A.R. Brown, D.M. de Leeuw, E.E. Havinga, A. Pomp, *Synth. Metals* **68** (1994) 65.

-
- ¹⁶ C. Tanase, E.J. Meijer, P.W.M. Blom, D.M. de Leeuw, *Org. Electron.* **4** (2003) 33.
- ¹⁷ F. Dinelli, M. Murgia, P. Levy, M. Cavallini, F. Biscarini, D.M. de Leeuw, *Phys. Rev. Lett.* **92** (2004) 116802.
- ¹⁸ K.P. Pernstich, S. Haas, D. Oberhoff, C. Goldmann, D.J. Gundlach, B. Batlogg, A.N. Rashid, G. Schitter, *J. Appl. Phys.* **96** (2004) 6431.
- ¹⁹ U. Zhokhavets, G. Gobsch, H. Hoppe, N.S. Sariciftci, *Synth. Metals* **143** (2004) 113.
- ²⁰ H.C.F. Martens, P.W.M. Blom, H.F.M. Schoo, *Phys. Rev. B* **61** (2000) 7489.